Journal of Medicinal Chemistry

pubs.acs.org/jmc

Article

Peripheral Selective Oxadiazolylphenyl Alanine Derivatives as Tryptophan Hydroxylase 1 Inhibitors for Obesity and Fatty Liver Disease

Eun Jung Bae,[#] Won Gun Choi,[#] Haushabhau S. Pagire, Suvarna H. Pagire, Saravanan Parameswaran, Jun-Ho Choi, Jihyeon Yoon, Won-il Choi, Ji Hun Lee, Jin Sook Song, Myung Ae Bae, Mijin Kim, Jae-Han Jeon, In-Kyu Lee, Hail Kim,* and Jin Hee Ahn*

Cite This: *J. Med. Chem.* 2021, 64, 1037−1053

Read Online

ACCESS | Metrics & More | Article Recommendations | Supporting Information

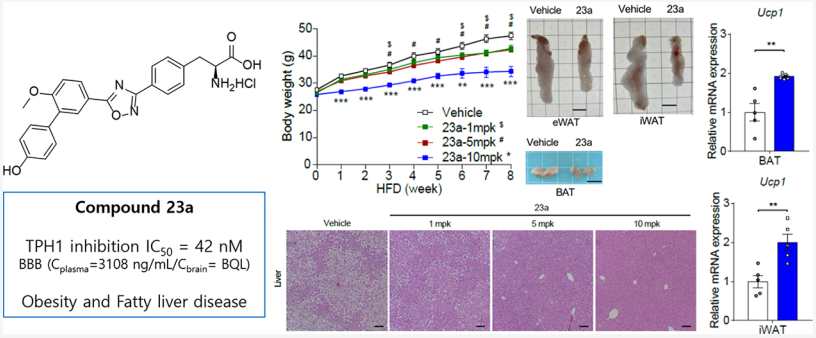

ABSTRACT: Tryptophan hydroxylase 1 (TPH1) has been recently suggested as a promising therapeutic target for treating obesity and fatty liver disease. A new series of 1,2,4-oxadiazolylphenyl alanine derivatives were identified as TPH1 inhibitors. Among them, compound **23a** was the most active in vitro, with an IC_{50} (half-maximal inhibitory concentration) value of 42 nM, showed good liver microsomal stability, and showed no significant inhibition of CYP and hERG. Compound **23a** inhibited TPH1 in the peripheral tissue with limited BBB penetration. In high-fat diet-fed mice, **23a** reduced body weight gain, body fat, and hepatic lipid accumulation. Also, **23a** improved glucose intolerance and energy expenditure. Taken together, compound **23a** shows promise as a therapeutic agent for the treatment of obesity and fatty liver diseases.

INTRODUCTION

Serotonin (5-hydroxytryptamine, 5-HT) is a monoamine found in the central and peripheral systems.[1−3] Serotonin is synthesized from L-tryptophan, sequentially, by the enzymes tryptophan hydroxylase (TPH) and aromatic amino acid decarboxylase (AAAD).[4,5] In serotonin biosynthesis, TPH is a rate-determining enzyme that catalyzes the hydroxylation of L-tryptophan[6,7] (Figure 1). Thus, serotonin production is controlled by the activity of TPH.[8]

In the central nervous system, serotonin acts as a neurotransmitter associated with mood, anxiety, cognition, and appetite and maintains homeostasis.[6,9,10] The lack of serotonin in the central nervous system (CNS) causes neuropsychiatric diseases.[11,12] In peripheral tissue, serotonin plays a critical role in the regulation of metabolism and is emerging as a potential target for treating both obesity and fatty liver disease.[13−16] Recently, our laboratory[17,18] and others found that high-fat diet (HFD)-fed TPH1 knockout (KO) mice showed reduced weight gain and lipogenesis in white adipose tissue (WAT), and increased thermogenesis in brown adipose tissue (BAT).[17,19−21] These results indicate that peripheral serotonin can contribute to weight gain and fat accumulation and that TPH1 inhibitors could serve as a new treatment for obesity and fatty liver disease.[17,20,22]

Serotonergic systems are divided into the central and peripheral systems by the blood−brain barrier (BBB).[23,24] As serotonin cannot cross the BBB,[24] two serotonergic systems are functionally separated. In this regard, we envisioned new peripheral TPH1 inhibitors that do not affect the CNS, for treating obesity and fatty liver disease.

Several TPH1 inhibitors have been reported previously. *p*-Chlorophenylalanine (pCPA) is one of the classic TPH1 inhibitors.[25,26] However, its binding activity to TPH1 in vitro is

Received: September 7, 2020
Published: January 8, 2021

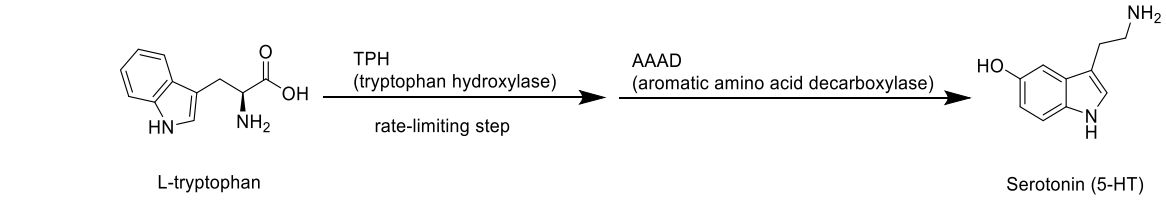

Figure 1. Biosynthesis of serotonin (5-hydroxytryptamine 5-HT) from L-tryptophan.

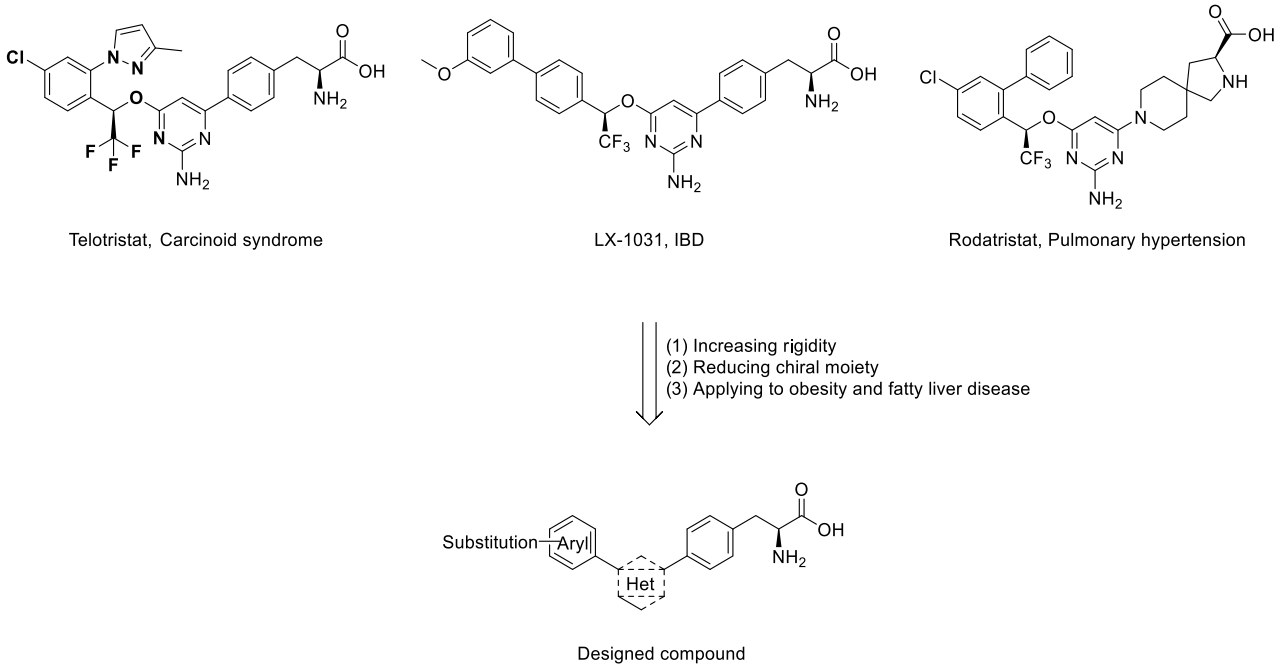

Figure 2. Drug design and reported TPH1 inhibitors in clinical trials (and market).

very weak (~50 μM of IC_{50} (half-maximal inhibitory concentration)), and pCPA is associated with central side effects including depression, because it passes into the CNS.[27−30] Lexicon Pharmaceuticals, Inc. reported a new class of phenyl alanine derivatives as a TPH1 inhibitor, using high-throughput screening.[31] Among them, telotristat ethyl, which is a prodrug of telotristat, was recently launched in the market as a TPH1 inhibitor for the treatment of carcinoid syndrome.[32−34] Karos Pharmaceuticals, Inc. reported a series of spirocyclic proline and acyl guanidine compound-based TPH1 inhibitors that were further modified from Lexicon's compound.[35,36] Phase I and II clinical trials are in progress for rodatristat ethyl for the treatment of pulmonary arterial hypertension (PAH).[37,38] In addition, the Novartis Research Foundation discovered a novel allosteric site binding TPH1 inhibitor, using a high-throughput proximity assay.[39] TPH1 inhibitors in clinical trials, such as telotristat, LX-1031, and rodatristat, share a chiral arylsubstituted trifluoroethoxyl group. These prompted us to design new TPH1 inhibitors, which have a less chiral center for ease of synthesis and more rigidity (Figure 2). Based on our previous TPH1 KO results for obesity and fatty liver[17] and reported effects of TPH1 inhibitors, we tried to develop our own new TPH1 inhibitor acting in the peripheral tissue for treating obesity and fatty liver disease. Here, we report the design, synthesis, and biological evaluation of a series of oxadiazolylphenyl alanine derivatives as TPH1 inhibitors.

RESULTS AND DISCUSSION

The synthetic route of 1,3-imidazole derivatives is outlined in Scheme 1. Commercially available L-tyrosine **1** was converted into ester **2**, followed by N-Boc protection with di-*tert*-butyl dicarbonate to give compound **3**. Compound **3** reacted with trifluromethanesulfonic anhydride to give triflate **4**.

Triflate **4** was treated with molybdenum hexacarbonyl in the presence of 1,1′-bis(diphenylphosphino)ferrocene in a microwave to give carboxylic acid **5**. The coupling of compound **5** with 2-bromo-1-(4-methoxyphenyl)ethan-1-one resulted in compound **6**. Cyclization of compound **6** with ammonium acetate provided intermediate **7**, followed by ester saponification and acidic deprotection to give the desired amino acid hydrochloride **8**.

1,3-Thidazole derivatives were prepared as described in Scheme 2. Triflate **4** was coupled with 4,4,4′,4′,5,5,5′,5′-octamethyl-2,2′-bi(1,3,2-dioxaborolane) in the presence of a palladium catalyst to yield boronate ester **9**. The Suzuki reaction of compound **9** with 2-bromothiazole gave intermediate **10**, which was further coupled with 1-bromo-4-methoxybenzene or 4-bromo-1,2-dimethoxybenzene in the presence of a palladium catalyst to afford **11a** or **11b**, respectively. Protected 1,3-thiazole **11** was hydrolyzed with a 2 M sodium hydroxide solution, followed by acidic deprotection to give the amino acid hydrochloride **12**.

1,2,4-Oxadiazole derivatives were synthesized as shown in Scheme 3. Commercially available (*S*)-2-amino-3-(4-cyanophenyl)propanoic acid **13** was converted into protected

https://dx.doi.org/10.1021/acs.jmedchem.0c01560
J. Med. Chem. 2021, 64, 1037−1053

Scheme 1. Synthesis of a 1,3-Imidazole Compound[a]

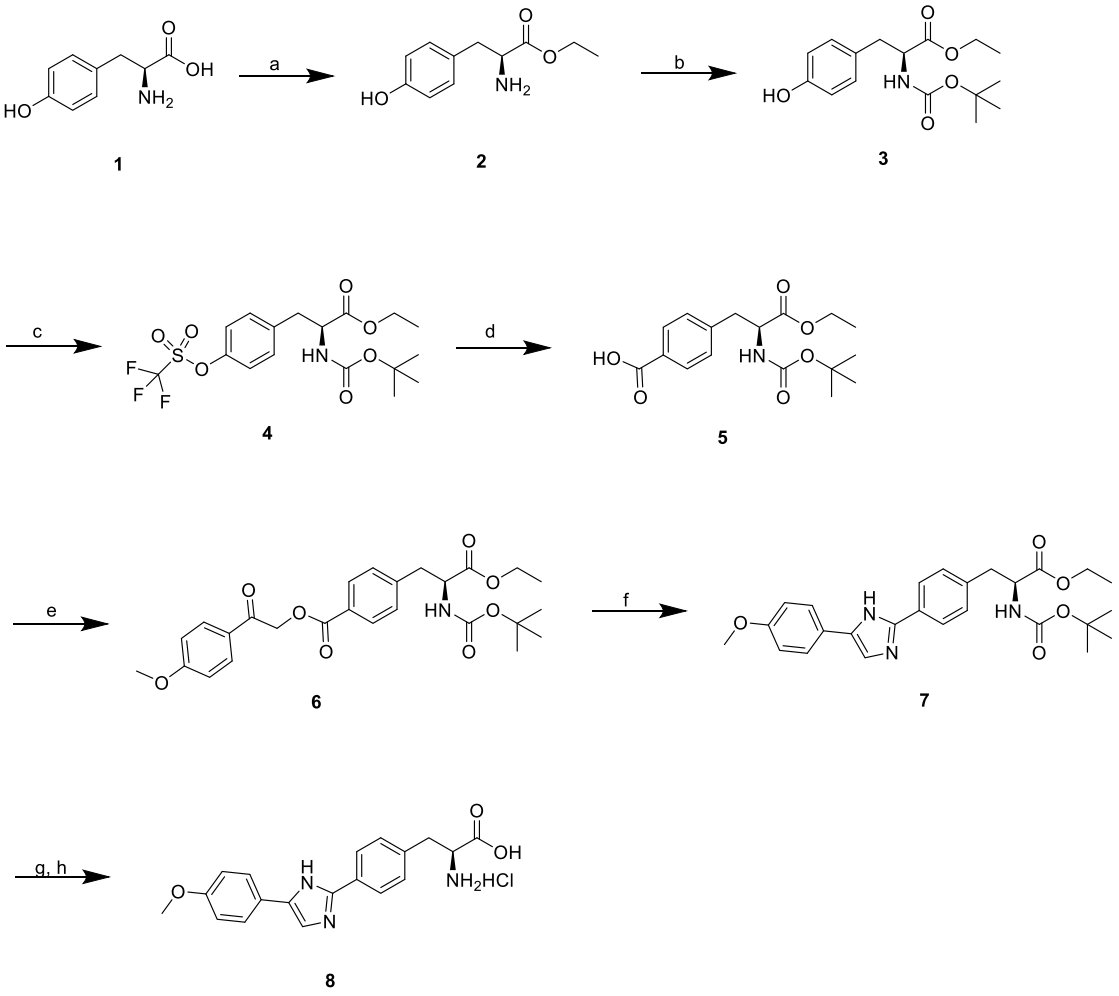

[a]Reagents and conditions: (a) $SOCl_2$, ethanol (EtOH), reflux, and 63%; (b) di-*tert*-butyl dicarbonate, Et_3N, methanol (MeOH), 0 °C to rt, and 96%; (c) trifluromethanesulfonic anhydride, pyridine, CH_2Cl_2, −15 °C to rt, and 83%; (d) $Mo(CO)_6$, *N*,*N*-diisopropylethylamine (DIPEA), 4-dimethylaminopyridine (4-DMAP), $Pd(OAc)_2$, 1,1′-bis(diphenylphosphino)ferrocene, 1,4-dioxane, H_2O, microwave, 110 °C, and 55%; (e) 2-bromo-1-(4-methoxyphenyl)ethan-1-one, Et_3N, acetonitrile, rt, and 78%; (f) ammonium acetate, xylene, 160 °C, and 15%; (g) NaOH, THF, H_2O, and rt; and (h) 4 M HCl in 1,4-dioxane, ethyl acetate (EtOAc), rt, and 68%.

compound **14**. Compound **14** was reacted with hydroxylamine hydrochloride under reflux to give intermediate **15**. Amidoxime **15** was coupled with substituted benzoic acid, followed by cyclization under reflux conditions to give compound **16**. Protected 1,2,4-oxadiazole **16** was treated with a 2 M sodium hydroxide solution, followed by acidic deprotection to give amino acid hydrochloride **17**.

Methyl 3-bromo-4-methoxybenzoate **18** was subjected to Suzuki reaction with substituted phenyl boronic acid in the presence of a palladium catalyst, followed by hydrolysis to give carboxylic acid **19**. Acetyl protection of compound **19** using acetyl chloride gave compound **20**. The amide coupling reaction of compound **22a** with ammonium hydroxide, followed by deprotection, resulted in compound **24**. Deacetylation of compound **21a** under basic conditions, followed by acidic deprotection, afforded compound **26**.

The synthesis of 1,3,4-oxadiazole derivatives is depicted in Scheme 4. 3-[Bis(dimethylamino)methyliumyl]-3*H*-benzotriazol-1-oxide hexafluorophosphate (HBTU) coupling of carboxylic acid **5** with substituted benzohydrazide produced compound **27**. Cyclization of compound **27** with *p*-toluenesulfonyl chloride gave compound **28**. Protected 1,3,4-oxadiazole **28** was hydrolyzed, followed by acidic deprotection to give amino acid hydrochloride **29**.

The preparation of 1,2,4-thiadiazole derivatives is outlined in Scheme 5. Commercially available 3-bromo-5-chloro-1,2,4-thiadiazole **31** was coupled with substituted 4-methoxyphenylboronic acid derivatives **30** in the presence of a palladium catalyst to produce compound **32**. Suzuki reaction of the bromide of compound **32** with boronate ester **9** provided compound **33**. Compound **33** was subjected to hydrolysis and acidic deprotection to afford 1,2,4-thiadiazole compound **34**.

To identify a new peripherally acting TPH1 inhibitor, we screened an in-house library with the amino acid moiety, which generally showed BBB impermeability. Compound **8**, containing a 1,3-imidazole core, was identified as a new and moderately potent TPH1 inhibitor (80% inhibition at 10 μM and 21% inhibition at 1 μM). We optimized the imidazole core and synthesized diverse five-membered heterocyclic derivatives, which are summarized in Table 1. LP533401 was used as a reference.[30] 1,3-Thiazole derivatives **12a** and **12b** showed decreased activities compared to compound **8**, with 10−15%

https://dx.doi.org/10.1021/acs.jmedchem.0c01560
J. Med. Chem. 2021, 64, 1037−1053

Scheme 2. Synthesis of a 1,3-Thiazole Compound[a]

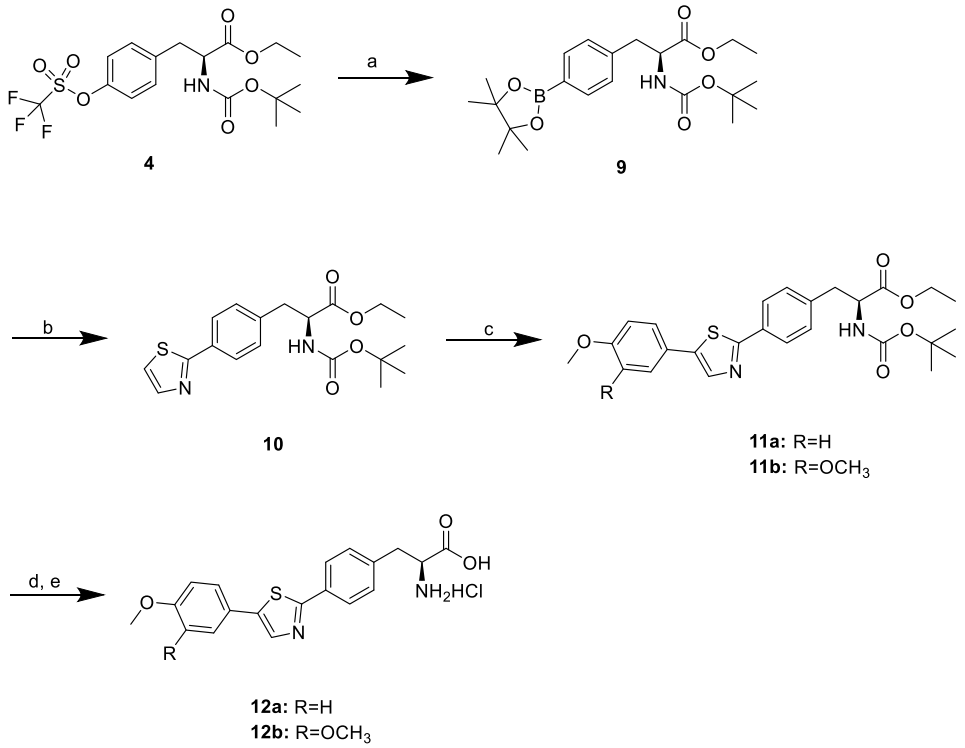

[a]Reagents and conditions: (a) 4,4,4′,4′,5,5,5′,5′-octamethyl-2,2′-bi(1,3,2-dioxaborolane), potassium acetate (KOAc), $PdCl_2(dppf).CH_2Cl_2$, DMSO, 100 °C, and 84%; (b) 2-bromothiazole, K_2CO_3, 5 mol % $Pd(PPh_3)_4$, 1,4-dioxane, H_2O, 100 °C, and 79%; (c) 1-bromo-4-methoxybenzene or 4-bromo-1,2-dimethoxybenzene, KOAc, $Pd(OAc)_2$, *N*-methyl-2-pyrrolidone (NMP), 120 °C, and 25−57%; (d) NaOH, THF, H_2O, rt; and (e) 4 M HCl in 1,4-dioxane, EtOAc, rt, and 23−69%.

inhibitions at 1 μM. 1,2,4-Oxadiazole derivatives (**17a**, **17f**) showed greatly increased in vitro inhibitory activity with compound **17f**, causing a 68% inhibition of TPH1 at 1 μM. However, once the 1,2,4-oxadiazole core was converted into a 1,3,4-oxadiazole core (**29a,b**), which is an isomer of 1,2,4-oxadiazole, the TPH1-inhibitory activity was lost (Table 1). Furthermore, the 1,2,4-thiadiazole core (**34a,b**) had a lower potency than the 1,2,4-oxadiazole core (**17a**, **17f**). Therefore, the 1,2,4-oxadiazole core **17a** was selected for further optimization.

As shown in Table 2, compound **17a** with a 4-methoxy group had good in vitro activity, with an IC_{50} value of 483 nM. However, the replacement of the 4-methoxy group with a simple phenyl group in **17b** resulted in the loss of inhibition. The replacement of the 4-methoxy group in **17a** with the 4-fluoro group in **17c** resulted in moderate activity, with an IC_{50} of 1570 nM. The replacement of the 4-methoxy moiety with 4-hydroxy in **17d**, or 3-methoxy in **17e**, resulted in no inhibitory activity at 1 μM. Compound **17f**, which has a 3,4-dimethoxy substituent, showed good in vitro activity, with an IC_{50} of 490 nM. This suggests that the 4-methoxy substituent is essential for in vitro activity and prompted us to modify the molecule at the 3-position. The 4-ethoxy substituent **17g** and the 4-methoxybenzyl derivative **17h** had reduced inhibitory activity. Therefore, we fixed the 4-methoxy substituent **17a** and further modified the molecule at the 3-position.

To optimize compound **17a** further, a molecular docking study of **17a** with TPH1 was conducted with the crystal structure of TPH1 (Protein Data Bank access code 3HF8),[40] and the compound's atomic coordinates were generated from its chemical structure. The docking calculations were carried out in AutoDock4.2.[41] The interactions between the inhibitor **17a** and TPH1 revealed that the binding mode of **17a** is similar to that of LP-533401, according to the PDB (Protein Data Bank) structure 3HF8,[40] and is shown in Figure 3. The amino acid head from the inhibitor **17a** interacts with Arg257 and Thr265 of TPH1, while the phenyl group attached to the amino acid head of **17a** has a $\pi-\pi$ interaction with His272. The core, 1,2,4-oxadiazole ring of inhibitor **17a** interacts with Glu317 of TPH1 via a π−anion interaction. The methoxyphenyl group has a $\pi-\pi$ T-shaped interaction with Tyr312 of TPH1. Docking analysis also revealed an unoccupied sub−pocket in residues 228 to 252 (forming a secondary structure of the β strand−α helix−β strand), while the distance between the 3-methoxy position on **17a** and the backbone oxygen of Gly234 of TPH1 was 8.17 Å, providing additional space for the optimization of **17a**. Based on the docking study and the activity of **17a** and **17f**, we further introduced substituents at the 3-methoxy position of **17a**.

Additional 4-methoxyphenyl-substituted 1,2,4-oxadiazole derivatives were synthesized and evaluated (Table 3). The introduction of a meta-substituted phenyl group (**17i**) at the compound **17a** resulted in a significant increase in the in vitro inhibitory activity (**17i**, 97% inhibition at 1 μM). We next introduced an electron-donating group on the meta-phenyl ring such as methoxy group **17j**, which resulted in extremely effective TPH1 inhibition (~100% inhibition at 1 μM), with an IC_{50} of 65 nM. The 4-hydroxy biphenyl analogue **23a** showed better in vitro activity than **17j** and telotristat (64 nM), with an IC_{50} of 42 nM.

https://dx.doi.org/10.1021/acs.jmedchem.0c01560
J. Med. Chem. 2021, 64, 1037−1053

Scheme 3. Synthesis of a 1,2,4-Oxadiazole Compound[a]

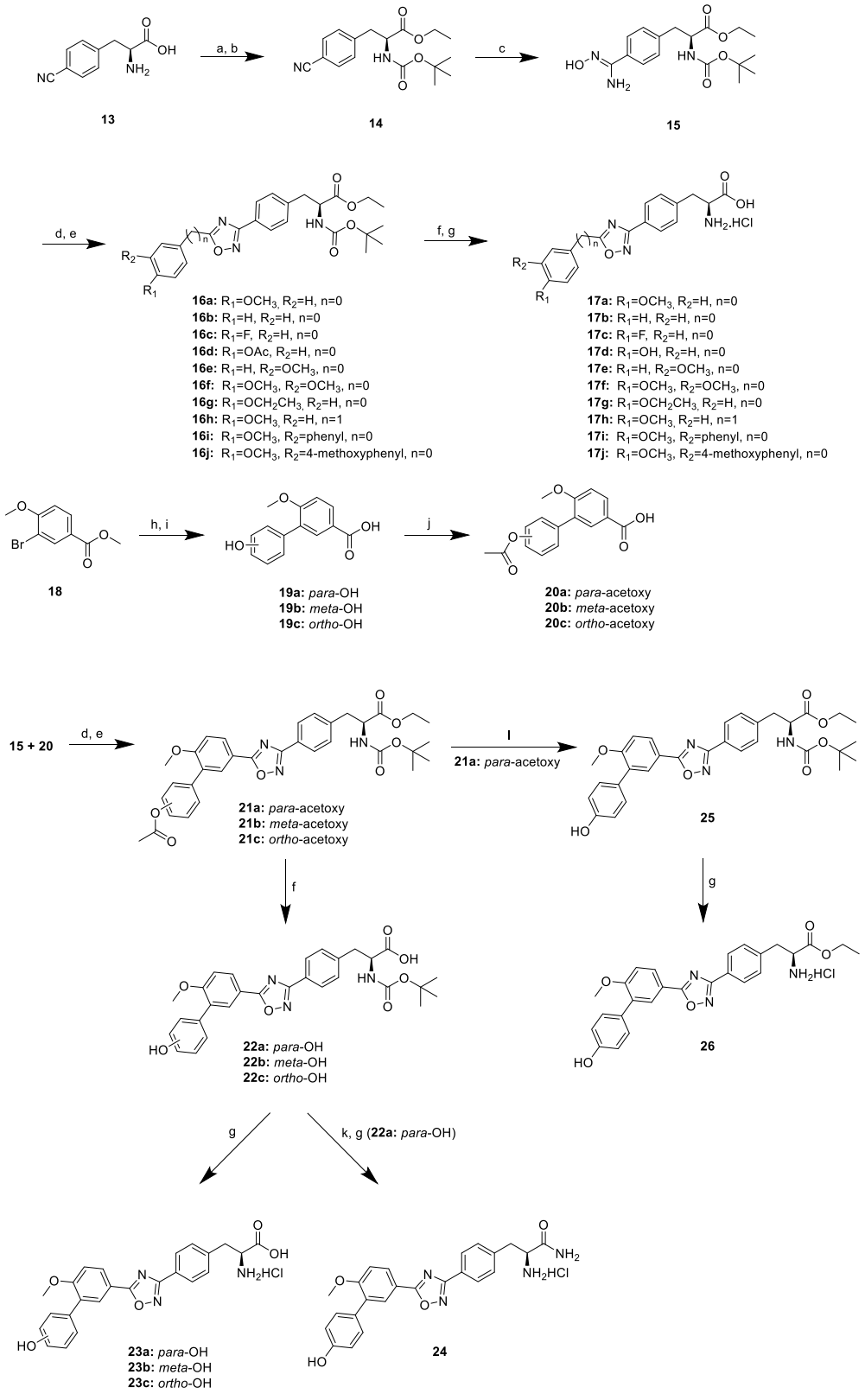

[a]Reagents and conditions: (a) di-*tert*-butyl dicarbonate, $NaHCO_3$, 1,4-dioxane, H_2O, 0 °C to rt, and 72%; (b) iodoethane, K_2CO_3, DMF, 0 °C to rt, and 94%; (c) hydroxylamine hydrochloride, Et_3N, EtOH, reflux, and 90%; (d) substituted benzoic acid, 1-ethyl-3-(3-dimethylaminopropyl)-carbodiimide, 1-hydroxybenzotriazole (HOBt), DIPEA, CH_2Cl_2, and rt; (e) 1,4-dioxane, reflux, 38−97%; (f) NaOH, THF, H_2O, and rt; (g) 4 M HCl in 1,4-dioxane, EtOAc, rt, and 26−94%; (h) substituted phenyl boronic acid, K_2CO_3, 5 mol % $Pd(PPh_3)_4$, 1,4-dioxane, H_2O, and 100 °C; (i) NaOH, THF, H_2O, rt, and 73−83%; (j) acetyl chloride, pyridine, CH_2Cl_2, 0 °C to rt, and 55−74%; (k) ammonium hydroxide, 1-ethyl-3-(3-diemthylaminopropyl)carbodiimide (EDCI), HOBt, THF, rt, and 35%; and (l) $NaHCO_3$, EtOH, rt, and 83%.

https://dx.doi.org/10.1021/acs.jmedchem.0c01560
J. Med. Chem. 2021, 64, 1037−1053

Scheme 4. Synthesis of a 1,3,4-Oxadiazole Compound[a]

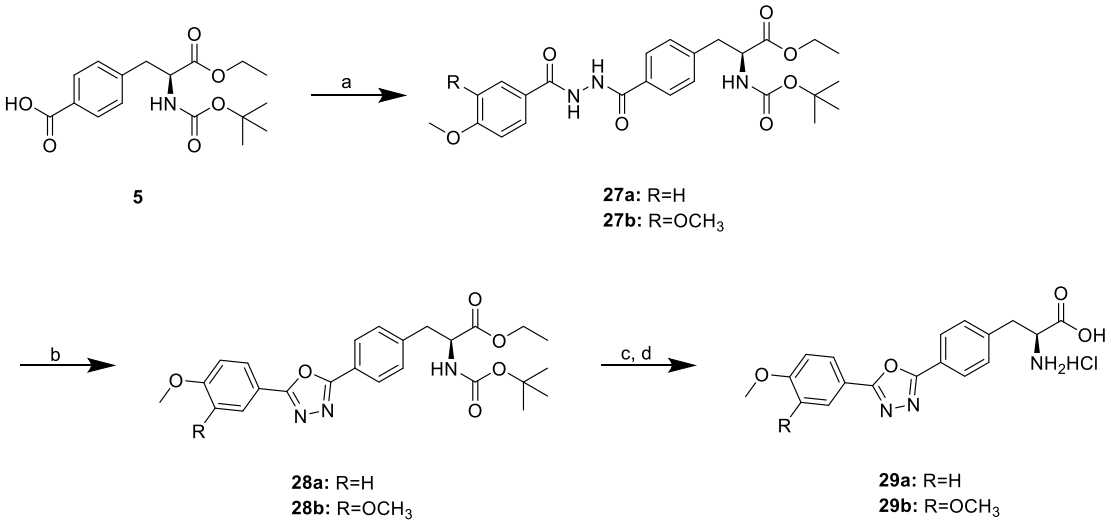

[a]Reagents and conditions: (a) 4-methoxybenzohydrazide or 3,4-dimethoxybenzohydrazide, HBTU, DIPEA, DMF, rt, and 92−97%; (b) DIPEA, *p*-toluenesulfonyl chloride, acetonitrile, rt, and 77−81%; (c) NaOH, THF, H_2O, and rt; and (d) 4 M HCl in 1,4-dioxane, EtOAc, rt, and 46−83%.

Scheme 5. Synthesis of a 1,2,4-Thiadiazole Compound[a]

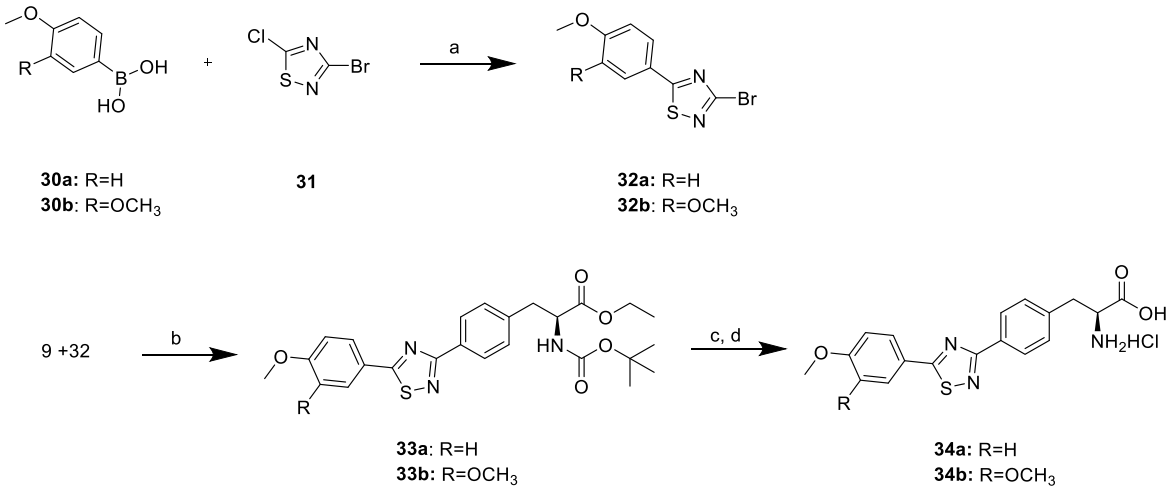

[a]Reagents and conditions: (a) tripotassium phosphate, $PdCl_2(dppf).CH_2Cl_2$, DMF, microwave, 80 °C, and 62−77%; (b) K_2CO_3, 5 mol % $Pd(PPh_3)_4$, 1,4-dioxane, H_2O, 100 °C, and 46−76%; (c) NaOH, THF, H_2O, and rt; and (j) 4 M HCl in 1,4-dioxane, EtOAc, rt, and 54−66%.

Next, we replaced the amino acid **23a** with amino amide **24**, its ethyl ester hydrochloride **26**, but this change resulted in the loss or decrease of TPH1 potency (Table 4).

We synthesized individual regioisomers of **23a** and evaluated their activity as shown in Table 5. Meta-hydroxy-substituted compounds (**23b**) and ortho-hydroxy-substituted compounds (**23c**) had weaker in vitro TPH1 inhibition activity as compared to that of para-substituted compounds (**23a**). In addition, compound **23d** had less in vitro potency than compound **23a**.

Based on the in vitro data, we chose compound **23a** as a prototype for further evaluation of its liver microsomal stability, and CYP and hERG inhibition (Table 6). Compound **23a** had good liver microsomal stability (92% of the parent remained after a 30 min incubation in human liver microsomes) and no significant CYP or hERG inhibition.

Further, the in vivo BBB permeability of **23a** was evaluated (Table 7). The concentration of **23a** was examined in brain tissue and plasma at 1 h after intraperitoneal (IP) administration (10 mg/kg). The concentration of **23a** in plasma was 3108.00 ± 1077.63 ng/mL, while it was below the quantification limit (31.3 ng/g) in the brain after 1 h. It indicates limited BBB penetration of compound **23a**.

It has been reported that genetic deletion or inhibition of TPH1 has an anti-obesity effect through the activation of thermogenesis in BAT and iWAT.[17−19] Thus, we evaluated the in vivo efficacy of compound **23a** for obesity and fatty liver disease. First, we checked 5-HT levels in serum and brain and whether **23a** has blood−brain barrier (BBB) permeability and affects 5-HT synthesis in the brain. C57BL6J mice were treated with **23a** or pCPA by a daily intraperitoneal injection for one week. Although pCPA treatment decreased 5-HT levels in both serum and brain, **23a** treatment decreased 5-HT levels only in serum but not in brain 5-HT (Figure 4A), indicating that **23a** cannot cross BBB and thereby effectively inhibits 5-HT synthesis only in peripheral tissues. To further verify the

https://dx.doi.org/10.1021/acs.jmedchem.0c01560
J. Med. Chem. 2021, 64, 1037−1053

Table 1. Structure−Activity Relationship of Five-Membered Heteroarylphenyl Alanine Derivatives

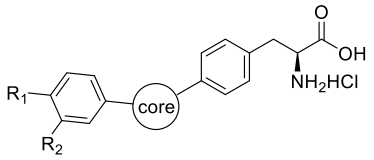

Compound	core	R_1	R_2	TPH1 % inhibition at 1 μM	TPH1 % inhibition at 10 μM
8	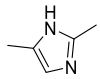	OCH_3	H	20.9%	80.3%
12a	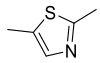	OCH_3	H	10 %	60.4%
12b	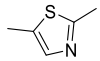	OCH_3	OCH_3	15%	63.7%
17a	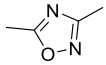	OCH_3	H	53 %	81.9%
17f	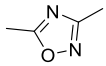	OCH_3	OCH_3	68 %	ND
29a	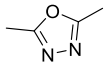	OCH_3	H	< 5 %	21.9%
29b	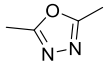	OCH_3	OCH_3	< 5 %	ND
34a	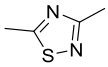	OCH_3	H	< 5 %	10.5%
34b	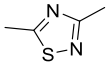	OCH_3	OCH_3	11.2%	19.1%
LP-533401	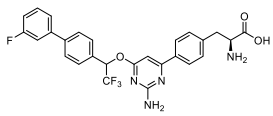			68 %	

anti-obesity effect of **23a** in vivo, C57BL6J mice were treated with **23a** by a daily intraperitoneal injection for eight weeks with a high-fat diet (HFD) feeding. After **23a** treatment for 8 weeks, serum 5-HT levels were robustly reduced (Figure 4B). Body weight gain upon HFD was attenuated in mice treated with **23a** compared to control mice (Figure 4C). The glucose tolerance test revealed that glucose tolerance was improved in HFD-fed mice treated with **23a** in a dose-dependent manner (Figure 4D). Furthermore, fat mass was decreased and lean body mass was increased by **23a** treatment (Figure 4E). Consistently, the size of adipose tissues including eWAT, iWAT, and BAT was reduced in **23a**-treated mice (Figure 4F−H). In the histological analysis using H&E staining, a crownlike structure was observed less in eWAT of **23a**-treated mice, indicating reduced adipose tissue inflammation (Figure 4I). In addition, adipocyte size in eWAT and iWAT was reduced in **23a**-treated mice (Figure 4I). In BAT, **23a** treatment decreased lipid droplet size and increased multilocular adipocytes after HFD feeding for eight weeks (Figure 4H,I). We further measured the metabolic rate using indirect calorimetry to check whether the anti-obesity effect of **23a** is attributed to the activation of brown fat. VO_2, VCO_2, and heat

https://dx.doi.org/10.1021/acs.jmedchem.0c01560
J. Med. Chem. 2021, 64, 1037−1053

Table 2. In Vitro Inhibitory Activity of 1,2,4-Oxadiazole Derivatives 17a−h Against TPH1

Compound	Structure	TPH1 inhibition (% inhibition at 1 μM)	IC_{50} (nM)
17a	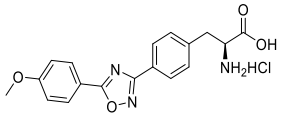	53 %	483 nM
17b	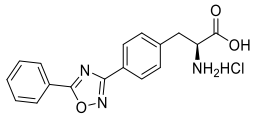	< 5 %	
17c	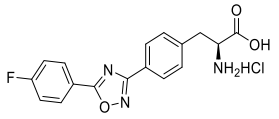	47 %	1570 nM
17d	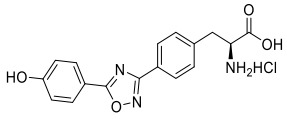	< 5 %	
17e	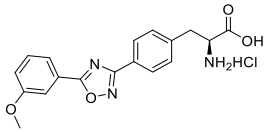	< 5 %	
17f	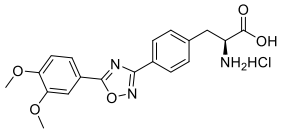	68 %	490 nM
17g	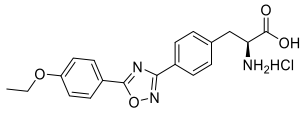	< 5 %	
17h	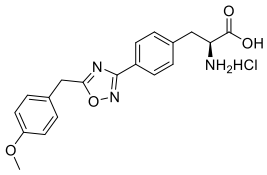	< 5 %	
LP533401		68 %	583 nM

production were increased in **23a**-treated mice (Figure 4J). However, RER of **23a**-treated mice was comparable to that of control mice, which suggested that **23a** treatment increased both glucose and lipid usage. To test thermogenic activity by **23a** treatment, we checked Uncoupling protein 1 (Ucp1) expression in both BAT and iWAT. Levels of *Ucp1* mRNA in BAT and iWAT were increased by **23a** treatment with HFD feeding, and immunohistochemical staining of UCP1 in BAT and iWAT showed the robust induction of UCP1 by **23a** treatment with HFD feeding in BAT but not in iWAT (Figure 4K−N). These data demonstrate that inhibition of 5-HT synthesis by **23a** treatment increases energy expenditure in BAT and thereby prevents obesity.

The inhibition of 5-HT synthesis is also known to reduce hepatic steatosis by reducing the hepatic lipogenesis through HTR2A in the liver.[42,43] Therefore, we confirmed the efficacy of **23a** for treating hepatic steatosis. Histological analysis revealed the robust reduction of hepatic lipid accumulation by **23a** treatment and, in accordance, hepatic triacylglycerol (TG) levels were reduced (Figure 4O,P). In addition, plasma TG and cholesterol levels were reduced in **23a**-treated HFD-fed mice (Figure 4Q,R). Taken together, these data indicate that

https://dx.doi.org/10.1021/acs.jmedchem.0c01560
J. Med. Chem. 2021, 64, 1037−1053

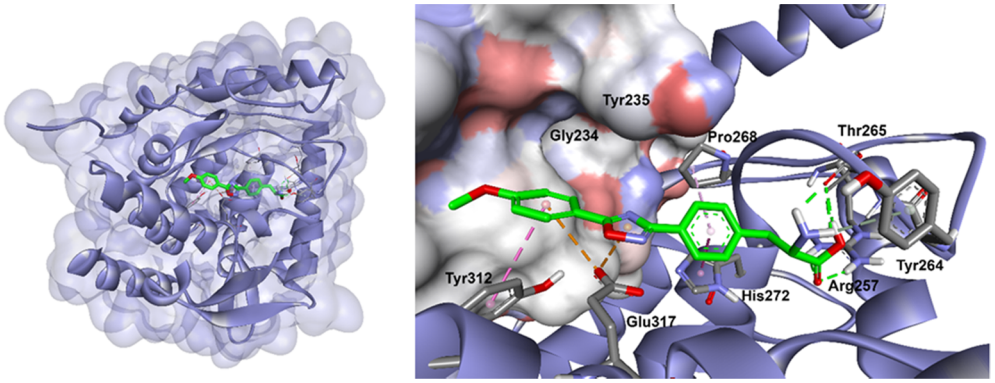

Figure 3. The predicted binding mode of compound **17a** at the inhibitor binding pocket of TPH1 has an orientation similar to that of LP-533401, according to the PDB structure, 3HF8.[40] The three-dimensional structure of human TPH1 is shown with a cartoon representation, whereas compound **17a** is shown as sticks. The unoccupied subpocket of the inhibitor binding pocket of TPH1 identified by docking analysis is shown with surface representation. The key interactions are depicted as dotted lines according to the interaction type.

Table 3. In Vitro Inhibitory Activity of Compounds 17a, 17i, 17j, and 23a against TPH1

Compound	Structure	TPH1 inhibition (% inhibition at 1 μM)	IC_{50} (nM)
17a	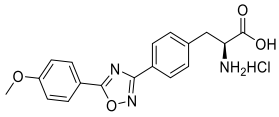	53 %	483 nM
17i	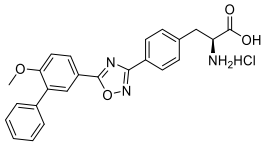	97%	166 nM
17j	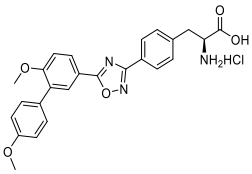	~100 %	65nM
23a	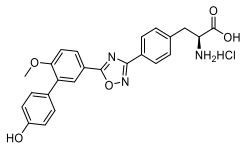	~100 %	42nM
LP533401		68 %	583 nM
Telotristat	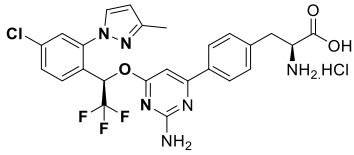	94 %	64 nM

23a can protect against diet-induced obesity and hepatic steatosis in vivo and thus it can be potentially used for anti-obesity and anti-fatty liver treatment.

The binding mode of **23a** with TPH1 was predicted using available structures of TPH1 (Figure 5). The amino acid head from the inhibitor **23a** interacts with Arg257, Thr265, and Ser336 via hydrogen bonds, as observed with LP-533401.[40] The phenyl group attached to the amino acid head of **23a** has a $\pi-\pi$ stacked interaction with Phe318 of TPH1. The 1,2,4-oxadiazole ring and the methoxyphenyl group of the inhibitor

https://dx.doi.org/10.1021/acs.jmedchem.0c01560
J. Med. Chem. 2021, 64, 1037−1053

Table 4. In Vitro Inhibitory Activities of Compounds 24 and 26 against TPH1

Compound	Structure	TPH1 inhibition (% inhibition at 1 μM)	IC_{50} (nM)
24	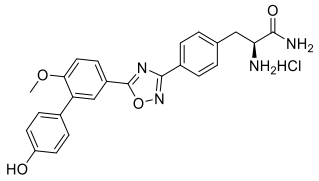	< 5 %	ND
26	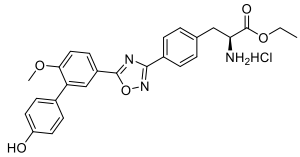	80.7%	120 nM
LP533401		68 %	583 nM

23a interact with Glu317 of TPH1 via a π−anion interaction. The hydroxyphenyl ring, which was introduced adjacent to the methoxyphenyl group in **23a**, has a hydrogen bond with Gly234 along with a $\pi-\pi$ interaction with Phe241 of TPH1, which is positioned in the subpocket, thereby enhancing the TPH1 inhibition effect of **23a**.

CONCLUSIONS

In this study, a series of 1,2,4-oxadiazolylphenyl alanine derivatives were identified and evaluated for their ability to inhibit TPH1 inhibitors. Among them, 1,2,4-oxadiazole derivatives with the 4-methoxyphenyl substituent were found to be potent TPH1 inhibitors. The binding mode of compound **17a** with TPH1 was predicted for further optimization. Compound **23a** was the most active in vitro, with an IC_{50} value of 42 nM, and showed good liver microsomal stability and no significant inhibitions of CYPs and hERG. Compound **23a** inhibited TPH1 in the peripheral tissue with limited BBB penetration. In high-fat diet-fed mice, **23a** reduced body weight gain and body fats, and improved glucose tolerance and energy expenditure. In addition, **23a** reduced hepatic lipid accumulation. Taken together, this newly developed peripheral TPH1 inhibitor can specifically inhibit the peripheral actions of 5-HT, and shows promise as a therapeutic agent to ameliorate obesity and fatty liver disease.

EXPERIMENTAL SECTION

General. All solvents and chemicals were used as purchased without further purification. All reported yields are isolated yields after column chromatography or crystallization. ^{1}H NMR spectra and ^{13}C spectra were recorded on a JEOL JNM-ECS400 spectrometer at 400 MHz for ^{1}H NMR and 100 MHz for ^{13}C NMR, respectively. The chemical shift (δ) is reported in ppm relative to tetramethylsilane (TMS) as an internal standard, and $CDCl_3$ and DMSO-*d* were used as solvents. Multiplicity of peaks is reported as s (singlet), d (doublet), t (triplet), q (quartet), dd (doublet of doublets), td (triplet of doublets), qd (quartet of doublets), dt (doublet of triplets), dq (doublet of quartets), ddd (doublet of doublets of doublets), and m (multiplet). Fast atom bombardment-high-resolution mass spectrometry (FAB-HRMS) data were obtained by a JMS 700 (JEOL, Japan). The purity of all tested compounds was ≥ 95%, as estimated by high-performance liquid chromatography (HPLC) analysis. Samples were analyzed on a Waters Agilent HPLC system equipped with a PDA detector and a Waters SB-C18 column (1.8 μm, 2.1 × 50 mm^2). The mobile phase was used with buffer A (ultrapure H_2O containing 0.1% TFA) and buffer B (chromatographic-grade CH_3CN). The flow rate was 0.5 mL/min.

(*S*)-2-amino-3-(4-(5-(4′-hydroxy-6-methoxy-[1,1′-biphenyl]-3-yl)-1,2,4-oxadiazol-3-yl)phenyl)propanoic Acid Hydrochloride (23a). *Step 1*. To a solution of (S)-amino-3-(4-cyanophenyl)-propanoic acid **13** (3.0 g, 15.77 mmol) in 1,4-dioxane (20 mL) at 0°C, $NaHCO_3$ (3.98 g, 47.32 mmol) in water (10 mL) was added. A solution of di-*tert*-butyl dicarbonate (5.16 g, 23.66 mmol) in 1,4-dioxane was added slowly to the reaction mixture at 0 °C over 1 h. The reaction mixture was allowed to reach room temperature and stirred for 18 h. After the completion of the reaction, the solvent was removed in vacuo. The remaining residue was dissolved in a solution of 5% $KHSO_4$ and the aqueous phase was extracted with ethyl acetate. The combined organic phase was dried over anhydrous sodium sulfate and the product was collected by filtration as a beige solid (3.31 g, 72%). ^{1}H NMR (400 MHz, DMSO-d_6) δ 12.72 (s, 1H), 7.75 (d, J = 8.2 Hz, 2H), 7.45 (d, J = 8.2 Hz, 2H), 6.81 (d, J = 7.9 Hz, 1H), 4.11−4.17 (m, 1H), 3.12 (dd, J = 13.7, 4.3 Hz, 1H), 2.89 (dd, J = 13.6, 10.8 Hz, 1H), 1.30 (s, 9H).

(*S*)-2-((*tert*-butoxycarbonyl)amino)-3-(4-cyanophenyl)propanoic acid (3.31 g, 11.40 mmol) and potassium carbonate (3.15 g, 22.80 mmol) were dissolved in DMF (10 mL), and the reaction mixture was cooled to 0 °C. Iodoethane (1.1 mL, 13.68 mmol) was slowly added to this mixture, and the reaction mixture was allowed to reach room temperature and stirred for 16 h. After the completion of the reaction, the mixture was diluted with ethyl acetate and water. The combined organic layer was washed with brine, dried over anhydrous sodium sulfate, and concentrated under the reduced pressure. The reaction mixture was purified by silica gel column chromatography to give ethyl (*S*)-2-((*tert*-butoxycarbonyl)amino)-3-(4-cyanophenyl)-propanoate **14** as a white solid (3.42 g, 94%). ^{1}H NMR (400 MHz, chloroform-*d*) δ 7.59 (d, J = 8.2 Hz, 2H), 7.27 (d, J = 8.2 Hz, 2H), 5.05 (d, J = 7.6 Hz, 1H), 4.58 (dd, J = 13.6, 6.4 Hz, 1H), 4.17 (q, J =

https://dx.doi.org/10.1021/acs.jmedchem.0c01560
J. Med. Chem. 2021, 64, 1037−1053

Table 5. In Vitro Inhibitory Activities of Compounds 23a–d against TPH1

Compound	Structure	TPH1 inhibition (% inhibition at 1 μM)	IC_{50} (nM)
23a	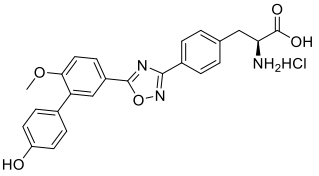	~100 %	42 nM
23b	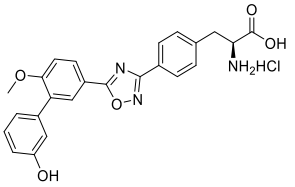	96.7%	60 nM
23c	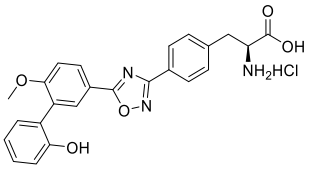	97.0 %	49 nM
23d	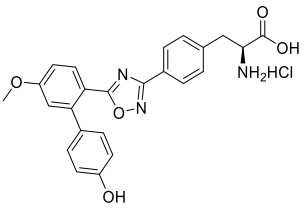	43.5 %	
LP533401		68 %	583 nM

Table 6. Liver Microsomal Stability, and CYP and hERG Inhibition of Compound 23a

assay	results
liver microsomal stability (rat)[a]	85% of the parent remained after a 30 min incubation
liver microsomal stability (human)	92% of the parent remained after a 30 min incubation
CYP inhibition	1A2: 3.2% inhibition at 10 μM
	2C9: <1% inhibition at 10 μM
	2C19: 6.7% inhibition at 20 μM
	2D6: <1% inhibition at 10 μM
	3A4: <1% inhibition at 10 μM
hERG inhibition	24.3% inhibition at 10 μM

[a]Buspirone was used as a positive control (0.1% (rat) and 4% (human) remained after a 30 min incubation).

Table 7. Brain/Plasma Concentration in Male ICR Mice (IP, 10 mg/kg, Mean ± SD, n = 3) for Compound 23a

	concentration (ng/mL or ng/g)	
Time (h)	plasma	brain tissue
1	3108.00 ± 1077.63	BQL[a]

[a]Below the quantification limit (31.3 ng/g).

7.1Hz, 2H), 3.14 (ddd, J = 53.7, 13.7, 6.1 Hz, 2H), 1.41 (s, 9H), 1.24 (t, J = 7.2 Hz, 3H).

Step 2. A mixture of ethyl (*S*)-2-((*tert*-butoxycarbonyl)amino)-3-(4-cyanophenyl)propanoate **14** (2.5 g, 7.85 mmol), hydroxylamine hydrochloride (1.64 g, 23.56 mmol), and triethylamine (5.48 mL, 39.26 mmol) in ethanol (20 mL) was stirred under reflux for 2 h. After the reaction mixture was cooled to room temperature, the volume was reduced by evaporation and water was added to the resulting mixture, followed by extraction with ethyl acetate. The combined organic phase was dried over anhydrous sodium sulfate, filtered, and evaporated in vacuo. The crude product was purified by silica gel column chromatography to give ethyl (*S*)-2-((*tert*-butoxycarbonyl)amino)-3-(4-(*N*-hydroxycarbamimidoyl)phenyl)-propanoate **15** (2.49 g, 90%) as a white solid. ^{1}H NMR (400 MHz, DMSO-d_6) δ 9.58 (s, 1H), 7.58 (d, J = 8.4 Hz, 2H), 7.32 (d, J = 8.0 Hz, 1H), 7.22 (d, J = 8.4 Hz, 2H), 5.77 (s, 2H), 4.10–4.16 (m, 1H), 4.07 (q, J = 7.1 Hz, 2H) 2.98 (dd, J = 13.7, 5.3 Hz, 1H), 2.86 (dd, J = 13.5, 10.1 Hz, 1H), 1.33 (s, 9H), 1.12 (t, J = 7.1 Hz, 3H).

Step 3. A mixture of methyl 3-bromo-4-methoxybenzoate **18** (3.9 g, 15.91 mmol), (4-hydroxyphenyl)boronic acid (2.41 g, 17.51 mmol), tetrakis(triphenylphosphine)palladium(0) (919.49 mg, 0.80

https://dx.doi.org/10.1021/acs.jmedchem.0c01560
J. Med. Chem. 2021, 64, 1037–1053

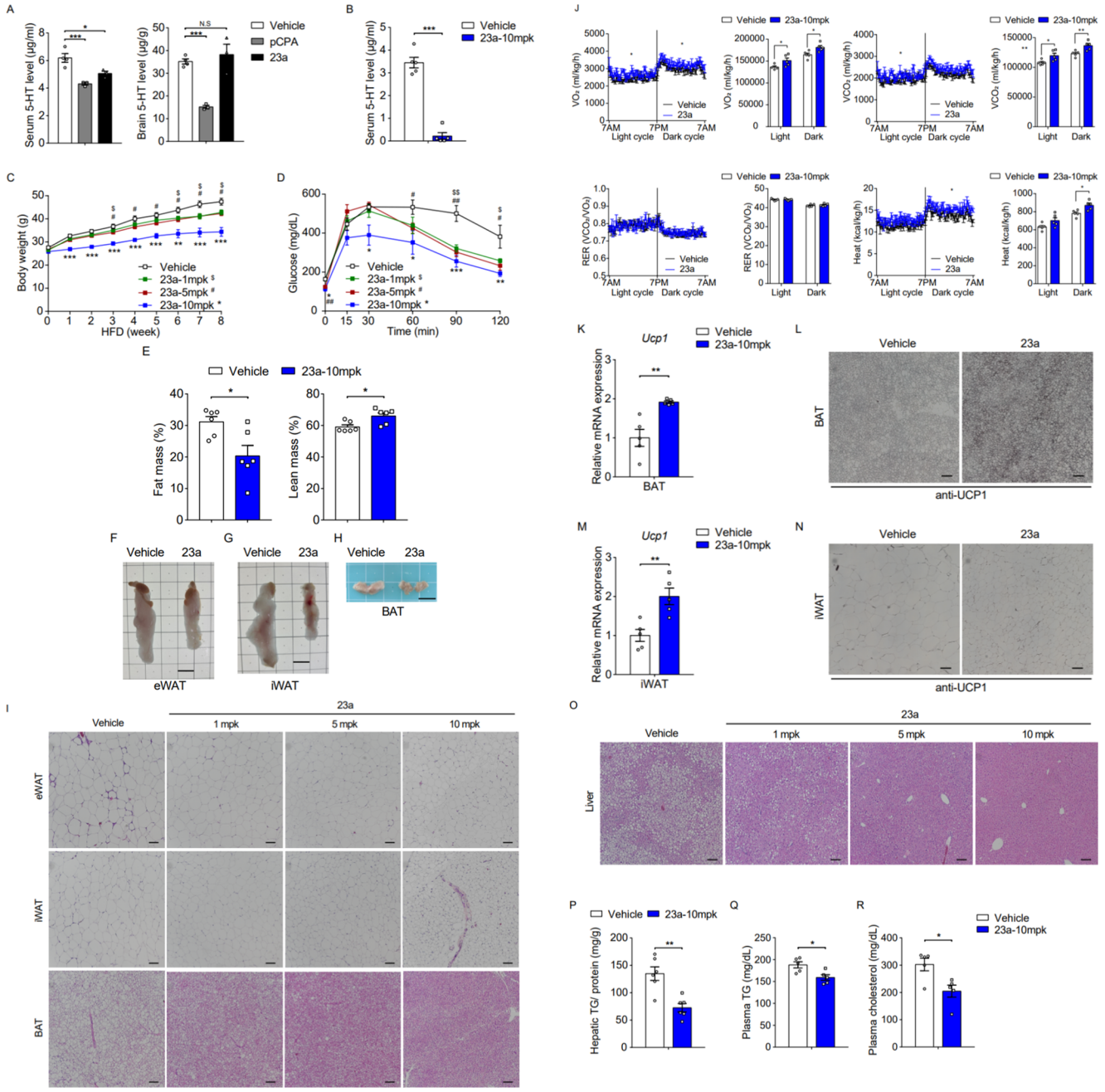

Figure 4. TPH1 inhibitor **23a** protects against diet-induced obesity in vivo in a mouse model by increasing energy expenditure via brown and beige adipose tissue activation. (A) Serum and brain 5-HT levels. Twelve week old mice treated with vehicle or pCPA (300 mg/kg) or **23a** (10 mg/kg) by a daily intraperitoneal injection with standard chow diet for one week (vehicle, n = 4/group; pCPA, *n* = 3/group; **23a**, *n* = 3/group). (B−R) Twelve week old mice were treated with vehicle or **23a** (1, 5, or 10 mg/kg) by a daily intraperitoneal injection with a high-fat diet for eight weeks. (B) Serum 5-HT levels of vehicle or 10 mg/kg **23a**-treated mice (n = 5/group). (C) Body weight curve during compound treatment with HFD (*n* = 6/group). (D) Intraperitoneal glucose tolerance test (IPGTT) after 16 hours of fasting (*n* = 6/group). (E) Percent fat mass and lean mass (*n* = 6/group). (F−H) Gross appearance of eWAT (F), iWAT (G), and BAT (H) with 10 mg/kg **23a** treatment. One block = 1 cm×1 cm. (I) Representative eWAT, iWAT, and BAT histology by H&E staining in vehicle- and **23a**-treated mice. Scale bars, 100 μm. (J) Metabolic parameters: oxygen (O_2) consumption, VO_2; carbon dioxide (CO_2) production, VCO_2; and heat production in vehicle or **23a**-treated mice (*n* = 5/group). (K and L) Relative mRNA expression of *Ucp1* (K) and immunohistochemical staining for UCP1 (L) in BAT of vehicle- and **23a**-treated mice (n = 5/group). Scale bars, 100 μm. (M and N) Relative mRNA expression of *Ucp1* (M) and immunohistochemical staining for UCP1 (N) in iWAT of vehicle- and **23a**-treated mice (*n* = 5/group). Scale bars, 100 μm. (O) Representative liver histology by H&E staining in vehicle- and **23a**-treated mice. Scale bars, 100 μm. (P) Hepatic TG levels (*n* = 6/group). (Q, R) Plasma TG (Q) and cholesterol (R) levels (n = 5/group). Data are expressed as means ± SEM. $^{\$}$, $^{\#}$, *P < 0.05, $^{\$\$}$, $^{\#\#}$, **P < 0.01, and $^{\$\$\$}$, $^{\#\#\#}$, ***P < 0.001. Student's *t*-test.

mmol), and a 2 M potassium carbonate solution (6.60 g, 47.74 mmol) in 1,4-dioxane (20 mL) was stirred for 2 h at 100 °C. After the reaction mixture was cooled to room temperature, the mixture was extracted with ethyl acetate and water. The organic phase was washed with brine. Then, the combined organic fraction was dried over anhydrous sodium sulfate and filtered. The solvent was removed under reduced pressure to afford a residue that was purified by silica gel column chromatography to give methyl 4′-hydroxy-6-methoxy-

https://dx.doi.org/10.1021/acs.jmedchem.0c01560
J. Med. Chem. 2021, 64, 1037−1053

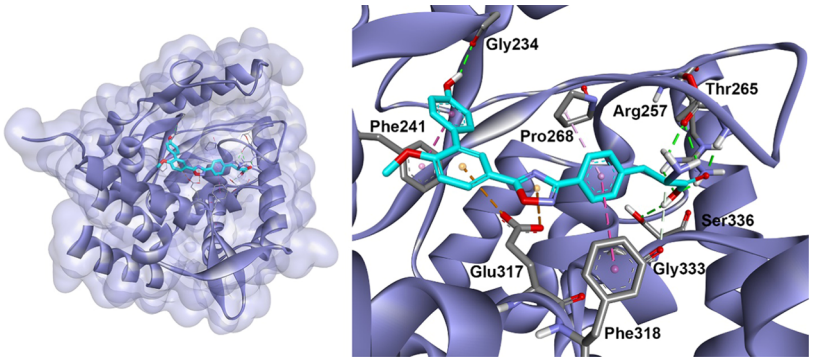

Figure 5. Compound **23a** binds at the inhibitor binding pocket of TPH1 with key interactions similar to those of compounds **17a** and LP-533401, according to the PDB structure, 3HF8.[40] The amino acid head and the 1,2,4-oxadiazole core of compound **23a** stabilize its binding with TPH1, while the introduced hydroxyphenyl ring enhances the inhibition effect of compound **23a**. The structure of human TPH1 is shown with a cartoon representation, whereas compound **23a** is shown as sticks. The key interactions are depicted as dotted lines according to the interaction type.

[1,1′-biphenyl]-3-carboxylate (2.875 g, 70%) as a white solid. ^{1}H NMR (400 MHz, chloroform-*d*) δ 8.01−7.98 (m, 2H), 7.41 (dt, *J* = 8.8, 2.4 Hz, 2H), 6.98 (dd, *J* = 5.0, 4.1 Hz, 1H), 6.91 (dt, *J* = 8.8, 2.4 Hz, 2H), 3.91 (s, 3H), 3.87 (s, 3H).

Methyl 4′-hydroxy-6-methoxy-[1,1′-biphenyl]-3-carboxylate (2.88 g, 11.13 mmol) in THF (20 mL) was treated with a 2 M sodium hydroxide solution. The reaction mixture was stirred for 16 h at ambient temperature. The solvent was removed in vacuo and the resulting solution was acidified with 1 N hydrochloric acid to pH 2. More water was added (50 mL) and the aqueous solution was extracted with ethyl acetate. The combined organic layer was washed with brine, dried over anhydrous sodium sulfate, and concentrated. The residue was purified by silica gel column chromatography to give 4′-hydroxy-6-methoxy-[1,1′-biphenyl]-3-carboxylic acid **19a** as a white solid (1.83 g, 67%). ^{1}H NMR (400 MHz, DMSO-d_6) δ 12.71 (s, 1H), 9.52 (s, 1H), 7.88 (dd, *J* = 8.7, 2.3 Hz, 1H), 7.77 (d, *J* = 2.4 Hz, 1H), 7.30 (dt, *J* = 9.3, 2.4 Hz, 2H), 7.16 (d, *J* = 8.9 Hz, 1H), 6.81 (dt, *J* = 9.2, 2.6 Hz, 2H), 3.83 (s, 3H).

Step 4. 4′-Hydroxy-6-methoxy-[1,1′-biphenyl]-3-carboxylic acid **19a** (1.83 g, 7.49 mmol) and pyridine (4.83 mL, 59.94 mmol) were dissolved in dichloromethane (20 mL) and the reaction mixture was cooled to 0 °C, and acetyl chloride (3.73 mL, 52.45 mmol) was added dropwise to this mixture. The reaction mixture was allowed to reach room temperature and stirred for 18 h. After the completion of the reaction, the mixture was diluted with dichloromethane and brine. The combined organic fraction was dried over anhydrous sodium sulfate, concentrated, and purified by silica gel column chromatography to give 4′-acetoxy-6-methoxy-[1,1′-biphenyl]-3-carboxylic acid **20a** as a white solid (1.185 g, 55%). ^{1}H NMR (400 MHz, chloroform-*d*) δ 8.10 (dd, *J* = 8.8, 2.3 Hz, 1H), 8.07 (d, *J* = 2.3 Hz, 1H), 7.55 (d, *J* = 8.4 Hz, 2H), 7.15 (d, *J* = 8.4 Hz, 2H), 7.03 (d, *J* = 8.8 Hz, 1H), 3.90 (s, 3H), 2.33 (s, 3H).

Step 5. A mixture of 4′-acetoxy-6-methoxy-[1,1′-biphenyl]-3-carboxylic acid **20a** (1.185 g, 4.139 mmol), ethyl (*S*)-2-((*tert*-butoxycarbonyl)amino)-3-(4-(*N*-hydroxycarbamimidoyl)phenyl)-propanoate **15** (1.75 g, 4.97 mmol), *N*-ethyl-*N*′-(3-dimethylaminopropyl)carbodiimide hydrochloride (1.98 g, 10.35 mmol), 1-hydroxybenzotriazole hydrate (950.78 mg, 6.21 mmol), and *N*,*N*-diisopropylethylamine (2.50 mL, 14.49 mmol) in dichloromethane (20 mL) was stirred for 18 h at ambient temperature. The reaction mixture was diluted with water and extracted with dichloromethane. The combined organic layer was dried over anhydrous sodium sulfate and evaporated. The residue was purified by silica gel chromatography to give ethyl (*S*)-3-(4-(*N*′-((4′-acetoxy-6-methoxy-[1,1′-biphenyl]-3-carbonyl)oxy)carbamimidoyl)phenyl)-2-((*tert*-butoxycarbonyl)amino)propanoate (2.45 g, 96%) as a white solid. ^{1}H NMR (400 MHz, chloroform-*d*) δ 8.11 (dd, *J* = 8.7, 2.3 Hz, 1H), 8.02 (d, *J* = 2.3 Hz, 1H), 7.70 (d, *J* = 8.2 Hz, 2H), 7.55 (dt, *J* = 9.2, 2.4 Hz, 2H), 7.21 (d, *J* = 8.2 Hz, 2H), 7.15 (dt, *J* = 9.0, 2.3 Hz, 2H), 7.04 (d, *J* = 8.7 Hz, 1H), 5.15 (s, 2H), 4.99 (d, *J* = 7.8 Hz, 1H), 4.57 (q, *J* = 6.4 Hz, 1H), 4.17 (q, *J* = 7.2 Hz, 2H), 3.89 (s, 3H), 3.14 (ddd, *J* = 31.4, 13.5, 5.7 Hz, 2H), 2.33 (s, 3H), 1.43 (s, 9H), 1.25 (t, *J* = 7.1 Hz, 3H).

(*S*)-3-(4-(*N*′-((4′-acetoxy-6-methoxy-[1,1′-biphenyl]-3-carbonyl)-oxy)carbamimidoyl)phenyl)-2-((*tert*-butoxycarbonyl)amino)-propanoate (2.45 g, 3.96 mmol) in 1,4-dioxane (10 mL) was heated to reflux for 18 h. After the reaction mixture was cooled to room temperature, the residue was extracted with ethyl acetate and water, and dried over anhydrous sodium sulfate. The reaction mixture was purified by silica gel column chromatography to give (*S*)-3-(4-(5-(4′-acetoxy-6-methoxy-[1,1′-biphenyl]-3-yl)-1,2,4-oxadiazol-3-yl)-phenyl)-2-((*tert*-butoxycarbonyl)amino)propanoate **21a** (1.94 g, 78%) as a white solid. ^{1}H NMR (400 MHz, chloroform-*d*) δ 8.19−8.16 (m, 2H), 8.09 (d, *J* = 8.4 Hz, 2H), 7.59 (dt, *J* = 9.2, 2.4 Hz, 2H), 7.29 (d, *J* = 8.4 Hz, 2H), 7.18 (dt, *J* = 9.2, 2.4 Hz, 2H), 7.11 (t, *J* = 4.6 Hz, 1H), 5.04 (d, *J* = 8.0 Hz, 1H), 4.61 (dd, *J* = 13.4, 6.4 Hz, 1H), 4.18 (q, *J* = 7.2 Hz, 2H), 3.92 (s, 3H), 3.17 (ddd, *J* = 26.6, 13.4, 6.0 Hz, 2H), 2.34 (s, 3H), 1.43 (s, 9H), 1.23 (d, *J* = 7.2 Hz, 3H).

Step 6. Ethyl (*S*)-3-(4-(5-(4′-acetoxy-6-methoxy-[1,1′-biphenyl]-3-yl)-1,2,4-oxadiazol-3-yl)phenyl)-2-((*tert*-butoxycarbonyl)amino)-propanoate **21a** (1.94 g, 3.23 mmol) in THF (20 mL) was treated with 2 M sodium hydroxide solution. The reaction mixture was stirred for 16 h at ambient temperature. The solvent was removed in vacuo and the resulting solution was acidified with 1 N hydrochloric acid to pH 3−4. The aqueous solution was extracted with ethyl acetate. The combined organic layer was washed with brine, dried over anhydrous sodium sulfate, and concentrated. The residue was purified by silica gel column chromatography to give (*S*)-2-((*tert*-butoxycarbonyl)-amino)-3-(4-(5-(4′-hydroxy-6-methoxy-[1,1′-biphenyl]-3-yl)-1,2,4-oxadiazol-3-yl)phenyl)propanoic acid **22a** (1.58 g, 92%) as a white solid. ^{1}H NMR (400 MHz, DMSO-d_6) δ 9.74 (s, 1H), 8.09 (dd, *J* = 8.7, 2.3 Hz, 1H), 7.96 (d, *J* = 2.1 Hz, 1H), 7.94 (d, *J* = 8.2 Hz, 2H), 7.39 (d, *J* = 4.9 Hz, 2H), 7.37 (d, *J* = 6.7 Hz, 2H), 7.32 (d, *J* = 8.9 Hz, 1H), 6.84 (dt, *J* = 9.3, 2.4 Hz, 2H), 6.50 (d, *J* = 3.4 Hz, 1H), 3.98 (td, *J* = 8.4, 4.9, 1H), 3.88 (s, 3H), 3.15 (dd, *J* = 13.4, 4.6 Hz, 1H), 2.97 (dd, *J* = 13.4, 7.6 Hz, 1H), 1.33 (s, 9H).

Step 7. To a solution of (*S*)-2-((*tert*-butoxycarbonyl)amino)-3-(4-(5-(4′-hydroxy-6-methoxy-[1,1′-biphenyl]-3-yl)-1,2,4-oxadiazol-3-yl)-phenyl)propanoic acid **22a** (600 mg, 1.13 mmol) in ethyl acetate (3 mL) was added a 4 M solution of hydrogen chloride in 1,4-dioxane (3 mL), and the reaction mixture was stirred for 12 h at ambient temperature. The mixture was concentrated and the residue was collected by filtration, and washed with ethyl acetate to afford (*S*)-2-amino-3-(4-(5-(4′-hydroxy-6-methoxy-[1,1′-biphenyl]-3-yl)-1,2,4-oxadiazol-3-yl)phenyl)propanoic acid hydrochloride **23a** (510 mg, 97%) as a white solid. ^{1}H NMR (400 MHz, DMSO-d_6) δ 9.62 (s, 1H), 8.44 (s, 3H), 8.12 (dd, *J* = 8.5, 2.1 Hz, 1H), 8.05 (d, *J* = 8.2 Hz, 2H), 7.99 (d, *J* = 2.4 Hz, 1H), 7.50 (d, *J* = 8.2 Hz, 2H), 7.38 (dt, *J* = 9.2, 2.3 Hz, 2H), 7.35 (d, *J* = 8.9 Hz, 1H), 6.86 (dt, *J* = 9.2, 2.3 Hz, 2H), 4.23 (t, *J* = 6.4 Hz, 1H), 3.89 (s, 3H), 3.22 (d, *J* = 6.4 Hz, 2H); ^{13}C NMR (100

https://dx.doi.org/10.1021/acs.jmedchem.0c01560
J. Med. Chem. 2021, 64, 1037−1053

MHz, DMSO-d_6) δ 175.35, 170.25, 168.03, 160.06, 157.20, 138.99, 130.97, 130.51, 130.43, 129.55, 128.48, 127.33, 127.13, 125.22, 115.79, 115.15, 112.52, 56.08, 53.12, 35.63; HRMS (FAB) m/z calculated for $C_{24}H_{22}N_3O_5$ $[M + H]^+$ 432.1559, found 432.1556; HPLC purity 100%.

In Vitro Screening Method. TPH1 enzyme activity was measured with a commercially available kit (BPS Bioscience). Compounds were dissolved in DMSO (Sigma). Then, 10 μL of the compound was dispensed into a 96-well microplate, and 40 μL of the TPH1 enzyme solution (320 ng enzyme/reaction) was added. Then, 50 μL of the TPH1 reaction solution was added, and the microplate was sealed with aluminum foil. The microplate was immediately cooled to 4 °C, gently shaken, and incubated for 4 hours. After a defined time, 10 μL of the TPH1 quench solution was added. Then, the fluorescence was measured with a Flexstation3 microplate reader at 300 nm for excitation and 360 nm for emission.

Blood–Brain Barrier (BBB) Penetration Study in Mice. Compound **23a** was evaluated for BBB penetration in male ICR mice as previously reported.[44] Male ICR mice were intraperitoneally administered **23a** at 10 mg/kg in a solution of DMSO/PEG400/saline = 5:40:55, v/v/v % (5 mL/kg). After 1 hour, the mice were euthanized using a CO_2 chamber, and blood from the heart was separated to plasma by centrifugation (13 000 rpm, 4 °C, 10 min). The remaining blood was washed out by performing cardiac perfusion with physiological saline containing 10 U/ml heparin. Then, the brain was removed from the skull and added to three volumes of PBS buffer per weight, homogenized, and kept at −20 °C until LC-MS/MS analysis for **23a**. The concentrations of **23a** were obtained in plasma and brain samples by an API 4000 Q trap mass spectrometer (Applied Biosystems, USA) coupled with a 1200 series HPLC system (Agilent, USA). Isocratic elution consisted of 80% acetonitrile and 20% water with 0.1% formic acid. The total run time was 3 minutes, and the flow rate was 0.3mL/min.

Animal Experiments. The experimental protocol for this study was approved by the Institutional Animal Care and Use Committee at the Korea Advanced Institute of Science and Technology. C57BL/6J mice were purchased from the Charles River Japan (Yokohama, Japan). The mice were housed in a specific pathogen-free barrier facility under a 12-h light−dark cycle. Food and water were provided ad libitum. At 12 weeks of age, mice were fed a high-fat diet (HFD, 60% fat calories) with vehicle or **23a** treatment by a daily intraperitoneal injection. Mice were euthanized by the method of cervical dislocation. The measurement of fluid, lean, and fat mass in live mice was performed by a body composition analyzer (LF50, Bruker). After 6 hours of fasting, mice were sacrificed and tissue samples were obtained.

Metabolic analysis. To measure the metabolic rate, the mice were housed individually in an eight-chamber, open-circuit Oxymax/CLAMS (Columbus Instruments Comprehensive Lab Animal Monitoring System) system. Each mouse was assessed for 72 h in the fed state to measure metabolic rates. The respiratory exchange ratio (RER = VCO_2/VO_2) and heat production (HP = (3.185 + 1.232 x RER) x VO_2) were calculated.

Histological Analysis. Epididymal, inguinal, brown adipose tissue, and liver were harvested, fixed in 4% (w/v) paraformaldehyde, and embedded in paraffin. Five-micron-thick tissue sections were deparaffinized, rehydrated, and stained with hematoxylin and eosin or used for immunohistochemistry, as described previously.[17]

Blood Profiling. Blood samples were obtained by cardiac puncture, and serum or plasma was isolated. Blood profiling was performed by GC Pharma (Green Cross Corporation). Plasma TG and cholesterol were detected with an in vitro enzymatic colorimetric assay (CHOL2 and TRIGL; Roche, Germany) using a Cobas 8000 clinical analyzer with a c702 module (Roche). Serum 5-HT was detected by LC-MS/MS (Liquid chromatography-tandem mass spectrometry) using a 5500 QTRAP LC-MS/MS system (AB SCIEX).

Quantification of Hepatic TGs. Liver tissues were homogenized in 5% NP-40 using FastPrep-24 (MP Biomedicals). TGs were solubilized by heating homogenates to 95 °C for 5 minutes and then cooling to 23 °C two times. Triglyceride reagent (Sigma-Aldrich) or PBS was added, and TGs were hydrolyzed into glycerol and free fatty acids by incubating samples at 37 °C for 30 minutes. Samples were incubated with Free Glycerol Reagent (Sigma-Aldrich) at 37 °C for 5 minutes for detecting hydrolyzed TG levels using a colorimetric assay. Differences in absorbance at 540 nm between hydrolyzed and nonhydrolyzed TGs were calculated using a glycerol standard (Sigma-Aldrich). The TG content was normalized to the protein concentration in homogenates, measured using a BCA Protein Assay Kit (Thermo Scientific).

Glucose Tolerance Tests. For the glucose tolerance test, overnight-fasted mice were intraperitoneally injected with 2 g/kg D-glucose (Sigma-Aldrich). Glucose concentrations were measured using a Gluco DR. TOP glucometer (Allmedicus, Korea).

Quantitative RT-PCR. TRIzol reagent (Ambion, USA) was used for total RNA extraction from harvested tissues. Complementary DNA was generated with the High Capacity cDNA Reverse Transcription kit (Applied Biosystems, Foster City, CA) from 1 μg of total RNA. Real-time qRT-PCR was performed with the Fast SYBR Green Master Mix (Applied Biosystems, Foster City, CA) and a ViiA 7 Real-Time PCR system (Applied Biosystems) according to the manufacturer's instructions. Expressional profiles were quantified based on the relative ddCt method with 36B4 as a reference gene.

Docking Studies of the Discovered Inhibitors with TPH1. The three-dimensional structure of discovered inhibitors was generated with ChemDraw and Chem3D, while the three-dimensional structure of TPH1 was obtained from the Protein Data Bank (Protein Data Bank access code 3HF8).[40] The structures of discovered inhibitors and TPH1 were preprocessed with Chem3D and Discovery Studio Visualizer, respectively, while the input structures for docking studies were generated with AutoDockTools with the standard protocol.[41] The docking calculations were performed with AutoDock4.2 of 200 Lamarckian genetic algorithm (LGA) runs, 300 initial population size, 100000000 evaluations along with 0.325 grid spacing, and 90x90x90 grid points focused on the inhibitor binding pocket deduced from LP-533401 binding. The rest of the parameters were set to default. The detailed docking methodology was described elsewhere.[45] The synthesized compounds were docked with the 3D structure of TPH1 as described in the methodology. Based upon the binding of the synthesized compounds, notably compound **17a**, the new compounds were synthesized. The docking poses and interactions of the discovered inhibitors with TPH1 were visualized in Discovery Studio Visualizer. They were created with Dassault Systèmes BIOVIA, Discovery Studio Visualizer, Dassault Systèmes: San Diego, 2002.

■ ASSOCIATED CONTENT

Supporting Information

The Supporting Information is available free of charge at https://pubs.acs.org/doi/10.1021/acs.jmedchem.0c01560.

Synthesis procedures; ^{1}H NMR, ^{13}C NMR, and HRMS spectra; and HPLC assessment of purity for all of the final compounds (PDF).

Molecular formula strings (CSV)

■ AUTHOR INFORMATION

Corresponding Authors

Hail Kim − *Graduate School of Medical Science and Engineering, Korea Advanced Institute of Science and Technology, Daejeon 34141, Republic of Korea*; Phone: +82-42-350-4243; Email: hailkim@kaist.edu; Fax: +82-42-350-4287

Jin Hee Ahn − *Department of Chemistry, Gwangju Institute of Science and Technology, Gwangju 61005, Republic of Korea*; orcid.org/0000-0002-6957-6062; Phone: +82-62-715-4621; Email: jhahn@gist.ac.kr

https://dx.doi.org/10.1021/acs.jmedchem.0c01560
J. Med. Chem. 2021, 64, 1037−1053

Authors

Eun Jung Bae − *Department of Chemistry, Gwangju Institute of Science and Technology, Gwangju 61005, Republic of Korea*

Won Gun Choi − *Graduate School of Medical Science and Engineering, Korea Advanced Institute of Science and Technology, Daejeon 34141, Republic of Korea*

Haushabhau S. Pagire − *Department of Chemistry, Gwangju Institute of Science and Technology, Gwangju 61005, Republic of Korea*

Suvarna H. Pagire − *Department of Chemistry, Gwangju Institute of Science and Technology, Gwangju 61005, Republic of Korea*

Saravanan Parameswaran − *Department of Chemistry, Gwangju Institute of Science and Technology, Gwangju 61005, Republic of Korea*

Jun-Ho Choi − *Department of Chemistry, Gwangju Institute of Science and Technology, Gwangju 61005, Republic of Korea;* orcid.org/0000-0001-5237-5566

Jihyeon Yoon − *Department of Chemistry, Gwangju Institute of Science and Technology, Gwangju 61005, Republic of Korea*

Won-il Choi − *Graduate School of Medical Science and Engineering, Korea Advanced Institute of Science and Technology, Daejeon 34141, Republic of Korea*

Ji Hun Lee − *Bio and Drug Discovery Division, Korea Research Institute of Chemical Technology, Daejeon 34114, Republic of Korea*

Jin Sook Song − *Bio and Drug Discovery Division, Korea Research Institute of Chemical Technology, Daejeon 34114, Republic of Korea*

Myung Ae Bae − *Bio and Drug Discovery Division, Korea Research Institute of Chemical Technology, Daejeon 34114, Republic of Korea*

Mijin Kim − *Research Institute of Aging and Metabolism, Kyungpook National University, Daegu 41404, Republic of Korea*

Jae-Han Jeon − *Research Institute of Aging and Metabolism, Kyungpook National University, Daegu 41404, Republic of Korea; Department of Internal Medicine, School of Medicine, Kyungpook National University, Kyungpook National University Hospital, Daegu 41944, Republic of Korea*

In-Kyu Lee − *Research Institute of Aging and Metabolism, Kyungpook National University, Daegu 41404, Republic of Korea; Department of Internal Medicine, School of Medicine, Kyungpook National University, Kyungpook National University Hospital, Daegu 41944, Republic of Korea*

Complete contact information is available at: https://pubs.acs.org/10.1021/acs.jmedchem.0c01560

Author Contributions

#E.J.B. and W.G.C. contributed equally to this work.

Notes

The authors declare no competing financial interest.

■ ACKNOWLEDGMENTS

This work was supported by grants from the Ministry of Science, ICT & Future Planning(MSIP)/National Research Foundation of Korea (NRF) (2016M3A9B6902868 and 2020M3A9E4038695), the Ministry of Trade, Industry and Energy (2020-10063396) and the Korea Health Industry Development Institute (KHIDI), funded by the Ministry of Health & Welfare (HI16C1501). We thank Jueun Kim and Hwajin Kim for their technical support.

■ ABBREVIATIONS

TPH, tryptophan hydroxylase; BBB, blood−brain barrier; PAH, pulmonary arterial hypertension; WAT, white adipose tissue; IC_{50}, half-maximal inhibitory concentration; BAT, brown adipose tissue; KO, knockout; HFD, high-fat diet; IPGTT, intraperitoneal glucose tolerance test; UCP1, uncoupling protein 1; MeOH, methanol; EtOH, ethanol; EtOAc, ethyl acetate; DIPEA, *N*,*N*-diisopropylethylamine; EDCI, 1-ethyl-3-(3-diemthylaminopropyl)carbodiimide; HOBt, hydroxybenzotriazole; 4-DMAP, 4-dimethylaminopyridine; KOAc, potassium acetate; NMP, *N*-methyl-2-pyrrolidone; HBTU, 3-[bis(dimethylamino)methyliumyl]-3*H*-benzotriazol-1-oxide hexafluorophosphate; IP, intraperitoneal; PDB, Protein Data Bank

■ REFERENCES

(1) Keszthelyi, D.; Troost, F. J.; Masclee, A. A. M. Understanding the Role of Tryptophan and Serotonin Metabolism in Gastrointestinal Function. *Neurogastroenterol. Motil.* **2009**, *21*, 1239−1249.

(2) Tecott, L. H. Serotonin and the Orchestration of Energy Balance. *Cell Metab.* **2007**, *6*, 352−361.

(3) Berger, M.; Gray, J. A.; Roth, B. L. The Expanded Biology of Serotonin. *Annu. Rev. Med.* **2009**, *60*, 355−366.

(4) Wang, L.; Erlandsen, H.; Haavik, J.; Knappskog, P. M.; Stevens, R. C. Three-Dimensional Structure of Human Tryptophan Hydroxylase and Its Implications for the Biosynthesis of the Neurotransmitters Serotonin and Melatonin. *Biochemistry* **2002**, *41*, 12569−12574.

(5) Young, S. N.; Gauthier, S.; Anderson, G. M.; Purdy, W. C. Tryptophan, 5-Hydroxyindoleacetic Acid and Indoleacetic Acid in Human Cerebrospinal Fluid: Interrelationships and the Influence of Age, Sex, Epilepsy and Anticonvulsant Drugs. *J. Neurol. Neurosurg. Psychiatry* **1980**, *43*, 438−445.

(6) Walther, D. J.; Peter, J. U.; Bashammakh, S.; Hörtnagl, H.; Voits, M.; Fink, H.; Bader, M. Synthesis of Serotonin by a Second Tryptophan Hydroxylase Isoform. *Science* **2003**, *299*, 76.

(7) Grahame-Smith, D. G. The Biosynthesis of 5-Hydroxytryptamine in Brain. *Biochem. J.* **1967**, *105*, 351−360.

(8) Amireault, P.; Sibon, D.; Coîté, F. Life without Peripheral Serotonin: Insights from Tryptophan Hydroxylase 1 Knockout Mice Reveal the Existence of Paracrine/Autocrine Serotonergic Networks. *ACS Chem. Neurosci.* **2013**, *4*, 64−71.

(9) Monti, J. M. Serotonin Control of Sleep-Wake Behavior. *Sleep Med. Rev.* **2011**, *15*, 269−281.

(10) Merens, W.; Willem Van der Does, A. J.; Spinhoven, P. The Effects of Serotonin Manipulations on Emotional Information Processing and Mood. *J. Affect. Disorder* **2007**, *103*, 43−62.

(11) Matthes, S.; Mosienko, V.; Bashammakh, S.; Alenina, N.; Bader, M. Tryptophan Hydroxylase as Novel Target for the Treatment of Depressive Disorders. *Pharmacology* **2010**, *85*, 95−109.

(12) Young, S. N.; Leyton, M. The Role of Serotonin in Human Mood and Social Interaction: Insight from Altered Tryptophan Levels. *Pharmacol. Biochem. Behav.* **2002**, *71*, 857−865.

(13) Namkung, J.; Kim, H.; Park, S. Peripheral Serotonin: A New Player in Systemic Energy Homeostasis. *Mol. Cells* **2015**, *38*, 1023−1028.

(14) Carey, A. L.; Kingwell, B. A. Reducing Peripheral Serotonin Turns up the Heat in Brown Fat. *Nat. Med.* **2015**, *21*, 114−116.

(15) Turner, N.; Kowalski, G. M.; Leslie, S. J.; Risis, S.; Yang, C.; Lee-Young, R. S.; Babb, J. R.; Meikle, P. J.; Lancaster, G. I.; Henstridge, D. C.; White, P. J.; Kraegen, E. W.; Marette, A.; Cooney, G. J.; Febbraio, M. A.; Bruce, C. R. Distinct Patterns of Tissue-Specific Lipid Accumulation during the Induction of Insulin

Resistance in Mice by High-Fat Feeding. *Diabetologia* **2013**, *56*, 1638−1648.
(16) Namkung, J.; Shong, K. E.; Kim, H.; Oh, C.; Park, S.; Kim, H. Inhibition of Serotonin Synthesis Induces Negative Hepatic Lipid Balance. *Diabetes Metab J.* **2018**, *42*, 233−243.
(17) Oh, C. M.; Namkung, J.; Go, Y.; Shong, K. E.; Kim, K.; Kim, H.; Park, B. Y.; Lee, H. W.; Jeon, Y. H.; Song, J.; Shong, M.; Yadav, V. K.; Karsenty, G.; Kajimura, S.; Lee, I. K.; Park, S.; Kim, H. Regulation of Systemic Energy Homeostasis by Serotonin in Adipose Tissues. *Nat. Commun.* **2015**, *6*, No. 6794.
(18) Shong, K. E.; Oh, C.-M.; Namkung, J.; Park, S.; Kim, H. Serotonin Regulates De Novo Lipogenesis in Adipose Tissues through Serotonin Receptor 2A. *Endocrinol. Metab.* **2020**, *35*, 470−479.
(19) Crane, J. D.; Palanivel, R.; Mottillo, E. P.; Bujak, A. L.; Wang, H.; Ford, R. J.; Collins, A.; Blümer, R. M.; Fullerton, M. D.; Yabut, J. M.; Kim, J. J.; Ghia, J. E.; Hamza, S. M.; Morrison, K. M.; Schertzer, J. D.; Dyck, J. R. B.; Khan, W. I.; Steinberg, G. R. Inhibiting Peripheral Serotonin Synthesis Reduces Obesity and Metabolic Dysfunction by Promoting Brown Adipose Tissue Thermogenesis. *Nat. Med.* **2015**, *21*, 166−172.
(20) Yabut, J. M.; Desjardins, E. M.; Chan, E. J.; Day, E. A.; Leroux, J. M.; Wang, B.; Crane, E. D.; Wong, W.; Morrison, K. M.; Crane, J. D.; Khan, W. I.; Steinberg, G. R. Genetic Deletion of Mast Cell Serotonin Synthesis Prevents the Development of Obesity and Insulin Resistance. *Nat. Commun.* **2020**, *11*, No. 463.
(21) Zhang, X.; Wang, X.; Yin, H.; Zhang, L.; Feng, A.; Zhang, Q. X.; Lin, Y.; Bao, B.; Hernandez, L. L.; Shi, G. P.; Liu, J. Functional Inactivation of Mast Cells Enhances Subcutaneous Adipose Tissue Browning in Mice. *Cell Rep.* **2019**, *28*, 792−803.
(22) Oh, C. M.; Park, S.; Kim, H. Serotonin as a New Therapeutic Target for Diabetes Mellitus and Obesity. *Diabetes Metab. J.* **2016**, *40*, 89−98.
(23) Chen, Y.; Liu, L. Modern Methods for Delivery of Drugs across the Blood-Brain Barrier. *Adv. Drug Delivery Rev.* **2012**, *64*, 640−665.
(24) Alexander, A.; Agrawal, M.; Uddin, A.; Siddique, S.; Shehata, A. M.; Shaker, M. A.; Rahman, S. A. U.; Abdul, M. I. M.; Shaker, M. A. Recent Expansions of Novel Strategies towards the Drug Targeting into the Brain. *Int. J. Nanomed.* **2019**, *14*, 5895−5909.
(25) Koe, B. K.; Weissman, A. P-Chlorophenylalanine: A Specific Depletor of Brain Serotonin. *J. Pharmacol. Exp. Ther.* **1966**, *154*, 499−516.
(26) Jäkälä, P.; Sirviö, J.; Jolkkonen, J.; Riekkinen, P.; Acsady, L.; Riekkinen, P. The Effects of P-Chlorophenylalanine-Induced Serotinin Synthesis Inhibition and Muscarinic Blockade on the Performance of Rats in a 5-Choice Serial Reaction Time Task. *Behav. Brain Res.* **1992**, *51*, 29−40.
(27) Liu, Q.; Yang, Q.; Sun, W.; Vogel, P.; Heydorn, W.; Yu, X. Q.; Hu, Z.; Yu, W.; Jonas, B.; Pineda, R.; Calderon-Gay, V.; Germann, M.; O'Neill, E.; Brommage, R.; Cullinan, E.; Platt, K.; Wilson, A.; Powell, D.; Sands, A.; Zambrowicz, B.; Shi, Z. C. Discovery and Characterization of Novel Tryptophan Hydroxylase Inhibitors That Selectively Inhibit Serotonin Synthesis in the Gastrointestinal Tract. *J. Pharmacol. Exp. Ther.* **2008**, *325*, 47−55.
(28) Engelman, K.; Lovenberg, W.; Sjoerdsma, A. Inhibition of Serotonin Synthesis by Para-Chlorophenylalanine in Patients with the Carcinoid Syndrome. *N. Engl. J. Med.* **1967**, *277*, 1103−1108.
(29) Alfieri, A. B.; Cubeddu, L. X. Treatment with Para-Chlorophenylalanine Antagonises the Emetic Response AND the Serotonin-Releasing Actions of Cisplatin in Cancer Patients. *Br. J. Cancer* **1995**, *71*, 629−632.
(30) Betari, N.; Sahlholm, K.; Ishizuka, Y.; Teigen, K.; Haavik, J. Discovery and Biological Characterization of a Novel Scaffold for Potent Inhibitors of Peripheral Serotonin Synthesis. *Future Med. Chem.* **2020**, *12*, 1461−1474.
(31) Shi, Z. C.; Devasagayaraj, A.; Gu, K.; Jin, H.; Marinelli, B.; Samala, L.; Scott, S.; Stouch, T.; Tunoori, A.; Wang, Y.; Zang, Y.; Zhang, C.; Kimball, S. D.; Main, A. J.; Sun, W.; Yang, Q.; Nouraldeen, A.; Yu, X. Q.; Buxton, E.; Patel, S.; Nguyen, N.; Swaffield, J.; Powell, D. R.; Wilson, A.; Liu, Q. Modulation of Peripheral Serotonin Levels by Novel Tryptophan Hydroxylase Inhibitors for the Potential Treatment of Functional Gastrointestinal Disorders. *J. Med. Chem.* **2008**, *51*, 3684−3687.
(32) Markham, A. Telotristat Ethyl: First Global Approval. *Drugs* **2017**, *77*, 793−798.
(33) Kulke, M. H.; Hörsch, D.; Caplin, M. E.; Anthony, L. B.; Bergsland, E.; Öberg, K.; Welin, S.; Warner, R. R. P.; Lombard-Bohas, C.; Kunz, P. L.; Grande, E.; Valle, J. W.; Fleming, D.; Lapuerta, P.; Banks, P.; Jackson, S.; Zambrowicz, B.; Sands, A. T.; Pavel, M. Telotristat Ethyl, a Tryptophan Hydroxylase Inhibitor for the Treatment of Carcinoid Syndrome. *J. Clin. Oncol.* **2017**, *35*, 14−23.
(34) Masab, M.; Saif, M. W. Telotristat Ethyl: Proof of Principle and the First Oral Agent in the Management of Well-Differentiated Metastatic Neuroendocrine Tumor and Carcinoid Syndrome Diarrhea. *Cancer Chemother. Pharmacol.* **2017**, *80*, 1055−1062.
(35) Goldberg, D. R.; De Lombaert, S.; Aiello, R.; Bourassa, P.; Barucci, N.; Zhang, Q.; Paralkar, V.; Stein, A. J.; Valentine, J.; Zavadoski, W. Discovery of Acyl Guanidine Tryptophan Hydroxylase-1 Inhibitors. *Bioorg. Med. Chem. Lett.* **2016**, *26*, 2855−2860.
(36) Goldberg, D. R.; De Lombaert, S.; Aiello, R.; Bourassa, P.; Barucci, N.; Zhang, Q.; Paralkar, V.; Valentine, J.; Zavadoski, W. Discovery of Spirocyclic Proline Tryptophan Hydroxylase-1 Inhibitors. *Bioorg. Med. Chem. Lett.* **2016**, *26*, 1124−1129.
(37) Goldberg, D. R.; De Lombaert, S.; Aiello, R.; Bourassa, P.; Barucci, N.; Zhang, Q.; Paralkar, V.; Stein, A. J.; Holt, M.; Valentine, J.; Zavadoski, W. Optimization of Spirocyclic Proline Tryptophan Hydroxylase-1 Inhibitors. *Bioorg. Med. Chem. Lett.* **2017**, *27*, 413−419.
(38) Aiello, R. J.; Bourassa, P. A.; Zhang, Q.; Dubins, J.; Goldberg, D. R.; De Lombaert, S.; Humbert, M.; Guignabert, C.; Cavasin, M. A.; McKinsey, T. A.; Paralkar, V. Tryptophan Hydroxylase 1 Inhibition Impacts Pulmonary Vascular Remodeling in Two Rat Models of Pulmonary Hypertension. *J. Pharmacol. Exp. Ther.* **2017**, *360*, 267−279.
(39) Petrassi, M.; Barber, R.; Be, C.; Beach, S.; Cox, B.; D'Souza, A. M.; Duggan, N.; Hussey, M.; Fox, R.; Hunt, P.; Jarai, G.; Kosaka, T.; Oakley, P.; Patel, V.; Press, N.; Rowlands, D.; Scheufler, C.; Schmidt, O.; Srinivas, H.; Turner, M.; Turner, R.; Westwick, J.; Wolfreys, A.; Pathan, N.; Watson, S.; Thomas, M. Identification of a Novel Allosteric Inhibitory Site on Tryptophan Hydroxylase 1 Enabling Unprecedented Selectivity over All Related Hydroxylases. *Front. Pharmacol.* **2017**, *8*, 1−12.
(40) Cianchetta, G.; Stouch, T.; Yu, W.; Shi, Z. C.; Tari, L. W.; Swanson, R. V.; Hunter, M. J.; Hoffman, I. D.; Liu, Q. Mechanism of Inhibition of Novel Tryptophan Hydroxylase Inhibitors Revealed by Co-Crystal Structures and Kinetic Analysis. *Curr. Chem. Genomics* **2010**, *4*, 19−26.
(41) Allouche, A. Software News and Updates Gabedit — A Graphical User Interface for Computational Chemistry Softwares. *J. Comput. Chem.* **2011**, *32*, 174−182.
(42) Choi, W.; Namkung, J.; Hwang, I.; Kim, H.; Lim, A.; Park, H. J.; Lee, H. W.; Han, K. H.; Park, S.; Jeong, J. S.; Bang, G.; Kim, Y. H.; Yadav, V. K.; Karsenty, G.; Ju, Y. S.; Choi, C.; Suh, J. M.; Park, J. Y.; Park, S.; Kim, H. Serotonin Signals through a Gut-Liver Axis to Regulate Hepatic Steatosis. *Nat. Commun.* **2018**, *9*, No. 4824.
(43) Kim, M.; Hwang, I.; Pagire, H. S.; Pagire, S. H.; Choi, W.; Choi, W. G.; Yoon, J.; Lee, W. M.; Song, J. S.; Yoo, E. K.; Lee, S. M.; Kim, M. J.; Bae, M. A.; Kim, D.; Lee, H.; Lee, E. Y.; Jeon, J. H.; Lee, I. K.; Kim, H.; Ahn, J. H. Design, Synthesis, and Biological Evaluation of New Peripheral 5HT2A Antagonists for Nonalcoholic Fatty Liver Disease. *J. Med. Chem.* **2020**, *63*, 4171−4182.
(44) Lee, J. H.; Bok, J. H.; Park, S. B.; Pagire, H. S.; Na, Y. J.; Rim, E.; Jung, W. H.; Song, J. S.; Kang, N. S.; Seo, H. W.; Jung, K. Y.; Lee, B. H.; Kim, K. Y.; Ahn, J. H. Optimization of Cyclic Sulfamide Derivatives as 11β-Hydroxysteroid Dehydrogenase 1 Inhibitors for the Potential Treatment of Ischemic Brain Injury. *Bioorg. Med. Chem. Lett.* **2020**, *30*, No. 126787.

https://dx.doi.org/10.1021/acs.jmedchem.0c01560
J. Med. Chem. 2021, 64, 1037−1053

(45) Parameswaran, S.; Saudagar, P.; Dubey, V. K.; Patra, S. Discovery of Novel Anti-Leishmanial Agents Targeting LdLip3 Lipase. *J. Mol. Graph. Model.* **2014**, *49*, 68−79.

https://dx.doi.org/10.1021/acs.jmedchem.0c01560
J. Med. Chem. 2021, 64, 1037−1053